

Luminous Signals of Inelastic Dark Matter in Large Detectors

Joshua Eby¹, Patrick J. Fox², Roni Harnik², and Graham D. Kribs³

¹Department of Particle Physics and Astrophysics,
Weizmann Institute of Science, Rehovot 76100, Israel

²Theoretical Physics Department, Fermilab, Batavia, IL 60510 USA

³Department of Physics, University of Oregon, Eugene, OR 97403 USA

Abstract

We study luminous dark matter signals in models with inelastic scattering. Dark matter χ_1 that scatters inelastically off elements in the Earth is kicked into an excited state χ_2 that can subsequently decay into a monoenergetic photon inside a detector. The photon signal exhibits large sidereal-daily modulation due to the daily rotation of the Earth and anisotropies in the problem: the dark matter wind comes from the direction of Cygnus due to the Sun's motion relative to the galaxy, and the rock overburden is anisotropic, as is the dark matter scattering angle. This allows outstanding separation of signal from backgrounds. We investigate the sensitivity of two classes of large underground detectors to this modulating photon line signal: large liquid scintillator neutrino experiments, including Borexino and JUNO, and the proposed large gaseous scintillator directional detection experiment CYGNUS. Borexino's (JUNO's) sensitivity exceeds the bounds from xenon experiments on inelastic nuclear recoil for mass splittings $\delta \gtrsim 240(180)$ keV, and is the *only* probe of inelastic dark matter for $350 \text{ keV} \lesssim \delta \lesssim 600 \text{ keV}$. CYGNUS's sensitivity is at least comparable to xenon experiments with $\sim 10 \text{ m}^3$ volume detector for $\delta \lesssim 150 \text{ keV}$, and could be substantially better with larger volumes and improved background rejection. Such improvements lead to the unusual situation that the inelastic signal becomes the superior way to search for dark matter even if the elastic and inelastic scattering cross sections are comparable.

1 Introduction

Inelastic dark matter [1–14] – where dark matter scatters off nuclei into an excited state – provides interesting new signals of dark matter. While originally motivated by the DAMA/LIBRA annual modulation [2, 3, 6, 9, 13, 15, 16], an inelastic dark matter explanation is now extremely difficult to reconcile with current data from several different experiments, despite valiant model building efforts [13, 17–22]. One of the appeals of inelastic dark matter is that it provides a rationale for why dark matter has not yet been seen in direct detection experiments. Models of inelastic dark matter typically involve an inelastic scattering cross section off nuclei that is much larger than the elastic cross section. Once the inelastic splitting is large, say $\delta \gtrsim 300$ keV, ordinary Z -exchange can mediate $\chi_1 + N \rightarrow \chi_2 + N$, and not be in violation of existing direct detection experimental bounds [14]. To probe large inelastic splittings it is critical to analyze high recoil events [14]. XENON100 [23] and PandaX [24] are already probing the inelastic frontier; however their sensitivity is rapidly diminished above about 300 keV due to the intrinsic limitation that the heaviest element on which the dark matter can inelastically scatter is xenon. This motivates new ideas to probe inelastic dark matter.

In this paper, we demonstrate that large underground neutrino detectors as well as large directional dark matter detectors can provide a new method to probe inelastic dark matter. Other proposed searches for dark matter that could yield a signal in neutrino detectors include dark matter that destroys target baryons [25–28], dark matter that yields annihilation or decay products detectable in these experiments [29–39], self-destructing dark matter [40], dark matter produced at high-intensity accelerators or radioactive sources [41], or dark matter bounced off energetic cosmic rays [41, 42].

Consider a dark matter particle with mass of order a TeV traversing through the Earth. This particle moves with the dark matter wind that appears in the Earth’s frame to be coming from the Cygnus constellation. If its speed is large enough, the dark matter can upscatter off a heavy nucleus (perhaps lead), into an excited state which could be several hundreds of keV heavier in mass. Had this upscattering been attempted off a xenon nucleus in one of the large direct detection experiments, it would have been kinematically inaccessible. The excited state continues in the same general direction, headed from Cygnus, for tens to hundreds of kilometers before decaying inside a large and clean detector, such as Borexino, JUNO, or the planned CYGNUS dark matter detectors. This type of signal exhibits a strong daily modulation because, when the detector is on the Cygnus-facing side of the Earth, there is far less “target material” available to upscatter. The mechanism is summarized, in cartoon form, in Fig. 1.

The signal we will consider thus consists of single photons with an energy equal to the mass splitting δ of inelastic dark matter and with a rate that exhibits a strong modulation with a period of a sidereal day. The shape and phase of the modulation is predicted and depends on the geographical location of the detector, allowing for excellent signal to background discrimination. The essential ingredients are: inelastic dark matter which is more massive than the target nucleus and mass splitting anywhere from the threshold of the detection experiment up to about 600 keV. The lifetime, ideally in the range of 0.1-10 seconds, is also crucial, but can arise naturally through a radiative decay.

Similar ingredients have been considered before in other contexts: Luminous Dark Matter [43]

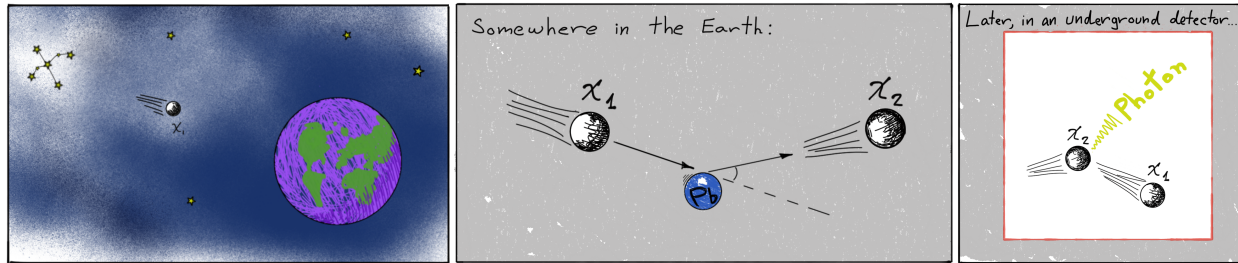


Figure 1: A cartoon summarizing the luminous dark matter signal discussed in this work. A heavy dark matter particle, χ_1 , is coming from the direction of the Cygnus constellation and approaching Earth with high speed (left). This allows it to upscatter off a (lead) nucleus somewhere within the Earth, deviating from its direction only slightly (middle). The excited state, χ_2 , decays back to χ_1 and a photon in an underground detector located on the opposite side of the Earth (right). The rate for this process would be much lower had the detector been on the Cygnus-facing side of the planet.

first proposed dark matter which upscatters to an excited state in the rock outside of a detector, and then decays into a photon that needed to be a few keV, with the goal of explaining the DAMA annual modulation. Alas, this novel DAMA explanation is ruled out by other direct detection experiments. Another idea, “dark matter in two easy steps” [11], proposed dark matter which upscatters into an excited state in lead shielding surrounding a neutrinoless double beta decay experiment, and then decays into a photon of order one hundred keV. This analysis shares some similarities with our paper: we both propose that inelastic dark matter is excited by lead outside of the detector volume, and propose looking for the photon from the decay of the excited state back into dark matter. Moreover, we both recognize that there is large sidereal-daily modulation of the rate that can be used to separate signal from background. The main differences between our analysis and theirs is: we utilize the entire Earth as upscatter material (focusing on upscatters off lead and iron); and, we consider a large range of photon energies between about 5-600 keV. The upper end of this range has the weakest constraints from direct detection experiments. The range 75-125 keV, which was the main focus of [11], is significantly constrained by PICO and the high recoil analysis of XENON100 [14]. Reinterpreting these bounds on the magnetic inelastic transition strength [14] implies the characteristic decay length of the excited state exceeds 50 (500) meters once $\delta \lesssim 150$ (100) keV. At these lengths, the gain from integrating over the trace lead abundance in the Earth is substantial in comparison to utilizing the close-in concentrated lead shielding of experiments sensitive to these photon energies.

In this paper we also decouple the upscatter process from the excited state decay. This is well-motivated, since there are many specific models that can have a large inelastic scattering rate, small elastic scattering rate, and excited state decay that all proceed through different processes. Examples include a variety of elementary candidates such as the wino and higgsino [44–47] as well as composite candidates [48]. The prototypical example model for this paper is the narrowly-split higgsino that arises from split Dirac supersymmetry [49]: in this model, the abundance of dark matter matches cosmological observations for $m_{\chi_1^0} \sim 1$ TeV; the neutral higgsino states $\chi_{1,2}^0$ are narrowly split by hundreds of keV; the dominant elastic scattering cross section is exceptionally small due to the twist-2 operator suppression as well as the cancellation against Higgs boson exchange

[46, 47]; and, the dominant decay of the excited (neutral) higgsino is indeed $\chi_2^0 \rightarrow \chi_1^0 \gamma$ [50]. But, we emphasize that none of these characteristics are unique to higgsinos – other models could easily yield similar outcomes.

What kind of detectors have the best sensitivity to photon line emission arising from the decay $\chi_2^0 \rightarrow \chi_1^0 \gamma$? Dark matter detectors can certainly be sensitive to this signal, and in fact they are designed to observe much smaller energy depositions. But, these direct detection experiments are smaller in size relative to their neutrino and directional dark matter detector counterparts, and they also have significant backgrounds when considering that there is only an electron-equivalent energy deposition from the photon. At xenon detectors, the background rate before cutting on a fiducial region is roughly at level of 0.1 events/kg/day/keVee [51, 52]. Within the fiducial region, the irreducible background from radioactive impurities (radon and krypton) is roughly 10^{-3} events/kg/day/keVee [53]. Borexino has a scintillator mass of 278 tons with a “background” rate of roughly 10^{-6} events/kg/day/keV [54]. For our purposes in this paper, background means the genuine radioactive background combined with the solar neutrino “background” (satisfying the common idiom that yesterday’s signal is today’s background). This low background rate does, however, rise rapidly for energy depositions below about 250 keV, where the signal must compete against a large background rate from ^{14}C β -decay, see Fig. 6.

It is clear that the particular material *within* the detector is not important so long as there is a high efficiency to absorb the photon from the excited state decay in order to generate a scintillation signal. Indeed, what maximizes our signal is the instrumented *volume* of a detector. This suggests large volume directional dark matter detectors which utilize a gaseous scintillator would be ideally suited to maximize the sensitivity to the photon deposition, if the backgrounds can be minimized. Certainly one obvious advantage of a gaseous scintillator is that its much-reduced density automatically reduces backgrounds from scattering, such as from solar neutrinos. Below we also discuss the opportunities for the proposed CYGNUS detector to probe the photon signal from inelastic dark matter.

2 Illuminating Inelastic Dark Matter

Inelastic dark matter is characterized by dark matter scattering off nuclei predominantly into an excited state with an elastic scattering rate below existing bounds. The range of inelastic splittings allowed by direct detection experiments that probed the nuclear recoil signal resulting from an inelastic collision was carried out in Ref. [14]. In this paper, our focus is on the detection of the excited state decay.

2.1 Model-independent requirements

Three basic requirements are needed to have a possibility of experimentally detecting excited state decay into dark matter:

1. Inelastic scattering $\chi_1 N \rightarrow \chi_2 N$ off (typically heavier) elements in the Earth has a sufficiently

large cross section to populate the flux of the excited state passing through a suitable detector.

2. The excited state decays frequently via $\chi_2 \rightarrow \chi_1\gamma$, with a lifetime that is long compared with the transit time through the detector, but not substantially longer than the transit time through the Earth.
3. Ordinary dark matter direct detection experimental bounds are satisfied. This constrains both (a) spin-independent elastic scattering, and (b) inelastic scattering off nuclei *within* a direct detection experiment.

In addition, if dark matter is heavier than the target nucleus, the upscattering yields an excited state that continues mainly in the forward direction, which results in a signal with a significant sidereal-daily modulation.

The requirement that the spin-independent elastic scattering be below current experimental bounds, item 3(a), is satisfied by a wide range of models. We have already mentioned the higgsino and wino as examples where the spin-independent elastic scattering cross section is very small [46, 47]. Composite dark matter candidates in this mass range can also have strong suppression if the leading spin-independent scattering interaction is an effective operator of high dimension, for example stealth dark matter that proceeds through the dimension-7 polarizability operator [55].

The model space is narrowed by the need to fulfill both requirement 1 and 3(b), namely that inelastic scattering off nuclei in the Earth has a sufficiently large cross section which, nevertheless, is not itself ruled out by inelastic scattering off the elements within a direct detection experiment. When $\delta \gtrsim 250$ keV, the bounds from direct detection experiments become highly suppressed by the very small fraction of the dark matter velocity distribution that can scatter (as well as the suppression from the nuclear form factor). In this region, inelastic dark matter can scatter much more easily off the heaviest trace elements in the Earth, and this provides a major lever-arm against direct detection bounds.

A second possibility, especially for smaller $\delta \lesssim 150$ keV, is that the inelastic cross section is itself very small. The advantage of considering such small δ is that there are lighter elements in the Earth, such as iron and silicon, that have a much larger number density. Here, a large underground experiment could have superior sensitivity over present direct detection experiments simply due to its (much) larger volume.

Finally, the requirement that the decay $\chi_2 \rightarrow \chi_1\gamma$ occurs frequently is not especially onerous. Kinematically there are only two possibilities in the Standard Model: the 2-body photon decay and the 3-body process $\chi_2 \rightarrow \chi_1\nu\bar{\nu}$. Phase space favors the photon decay, though a model-dependent calculation is needed to determine which process actually dominates. We shall see that in an interesting class of models this is indeed the case and that the lifetime is also in the interesting range. We note that if a light mediator with mass less than δ is also present in the model, then additional decay modes can be present.

2.2 Narrowly-split higgsinos

The reader may find it helpful to have a concrete model in mind while considering our model-independent results below. For this, the narrowly-split higgsino, which we describe below, provides a great example. For a recent review of the experimental status of the narrowly-split Higgsino, see [56]. Readers who have no appetite for models in these data-driven times may move on to the next section.

Higgsinos are spin-1/2 superpartners of the two Higgs doublets in the minimal supersymmetric standard model [57]. In the limit that all of the superpartners are heavy, the higgsino spectrum is characterized by

$$\begin{aligned}
 m_\chi &\simeq |\mu| \\
 m_{\chi^\pm} - m_{\chi^0} &\simeq \left(1 + \frac{1}{\cos\theta_W}\right) \alpha_2 m_W \sin^2\left(\frac{\theta_W}{2}\right) \\
 m_{\chi_2^0} - m_{\chi_1^0} &\simeq m_Z^2 \left(\frac{\sin^2\theta_W}{M_1} + \frac{\cos^2\theta_W}{M_2}\right)
 \end{aligned} \tag{1}$$

where μ is the higgsino mass and $M_{1,2} \gg |\mu|$ are the Majorana masses for the bino and wino [49, 58]. It is well known that the higgsino dark matter relic abundance matches cosmology when $|\mu| \simeq 1.1$ TeV. This mass scale is obviously above the mass of the heaviest nucleus we consider in this paper (lead), consistent with maximizing the inelastic scattering rate. A narrow splitting $\delta = m_{\chi_2} - m_{\chi_1} \lesssim 800$ keV between the neutral higgsinos occurs when $M_{1,2} \gtrsim 10^7$ GeV. The large splitting between the higgsino mass and the electroweak gauginos could arise naturally as a one-loop radiative correction from a heavy bino [49]. The elastic scattering cross section is highly suppressed, $\sigma_{\chi_1 n} \lesssim 10^{-48}$ cm², due to the twist-2 operator suppression as well as the partial cancellation against Higgs boson exchange [46, 47]. The excited state neutral higgsino has a one-loop radiative decay with width (in the limit where all other superpartners are decoupled [50])

$$\Gamma_{\chi_2 \rightarrow \chi_1 \gamma} \simeq \alpha_{\text{em}} \alpha_W^2 \frac{\delta^3}{4\pi^2 m_1^2} \tag{2}$$

that leads to a characteristic decay length of

$$\ell_{\chi_2} = \frac{cv}{\Gamma_{\chi_2 \rightarrow \chi_1 \gamma}} = 20 \text{ km} \left(\frac{cv}{400 \text{ km/s}}\right) \left(\frac{400 \text{ keV}}{\delta}\right)^3 \left(\frac{m_1}{1 \text{ TeV}}\right)^2, \tag{3}$$

where $m_{(1,2)} = m_{\chi_{(1,2)}}$. The photon decay can be compared with the 3-body process mediated by the weak interaction

$$\Gamma_{\chi_2 \rightarrow \chi_1 \nu \bar{\nu}} \sim \alpha_W^2 \frac{\delta^5}{120 \cos^4\theta_W \pi m_Z^4}. \tag{4}$$

The photon decay dominates provided

$$\left(\frac{\delta}{1 \text{ GeV}}\right)^2 \left(\frac{m_1}{1 \text{ TeV}}\right)^2 \lesssim 1. \tag{5}$$

This is clearly satisfied throughout the inelastic parameter space that we consider in this paper.

Finally, the inelastic transition $\chi_1 N \rightarrow \chi_2 N$ is mediated by Z -exchange for the higgsino that (famously) has a per nucleon cross section $\sigma_0 \sim 10^{-39} \text{ cm}^2$, before kinematic suppression from phase space and nuclear form factors are taken into account. Once $\delta \gtrsim 300 \text{ keV}$, direct detection experimental bounds are satisfied [23, 24, 48]. In the narrowly-split higgsino model, the inelastic transition proceeds through Z -exchange, and so therefore the inelastic cross section is fixed. If we generalize beyond Z -exchange, or allow $|\mu|$ to take values somewhat smaller or larger than the relic abundance would suggest, there is larger range of the inelastic scattering cross section that could be considered. As we will see, the detection of photons in large underground neutrino experiments will extend the reach for inelastic dark matter to both larger inelastic splittings as well as cross sections that are considerably smaller than Z -exchange.

For the remainder of the paper, we assume a model-independent spin-independent inelastic scattering cross section σ_0 (not necessarily Z -exchange) with an excited state decay rate given by Eq. (2).

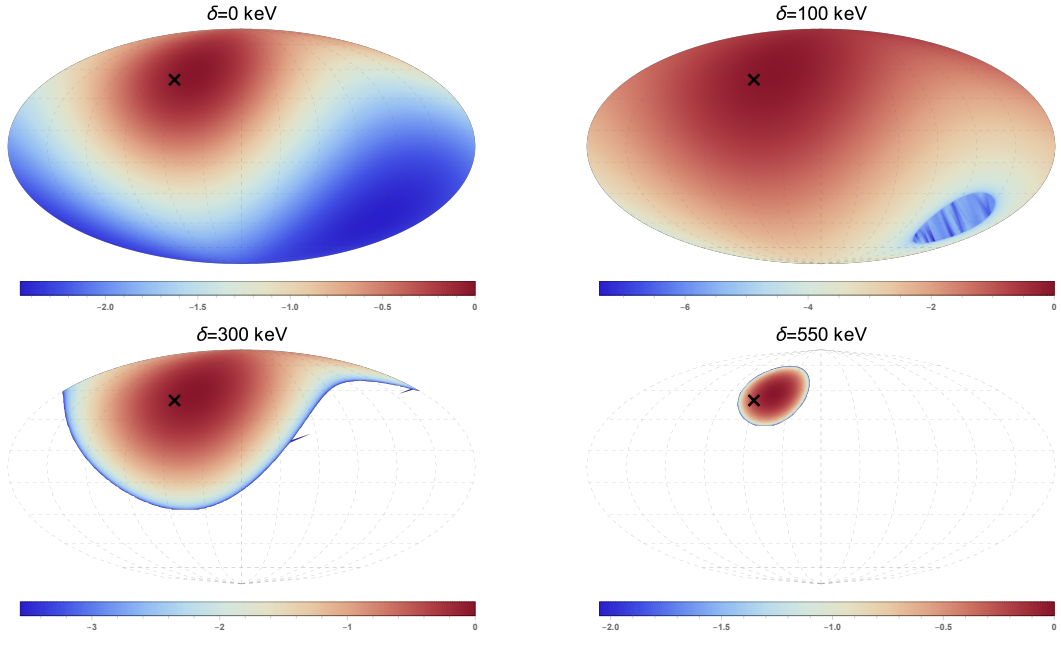
3 Luminous Signals and Sidereal Daily Modulation

In this section we discuss the luminous dark matter signals in inelastic models and show that the signal rate modulates strongly with a period of one sidereal day. The modulation is the result of a convolution of three anisotropic effects, which will be discussed in the upcoming three subsections: the anisotropy of high-speed dark matter, the anisotropy of the rock overburden in the lab, and the anisotropy of the upscattering of heavy dark matter in the Earth.

3.1 Anisotropy of high speed dark matter

It is well known [59] that the motion of the Sun/Earth system in the galaxy causes the dark matter wind to head towards us from a direction that approximately aligns with the location of the Cygnus constellation. Yet, dark matter impinging the Earth is not unidirectional, since the velocity distribution of dark matter in the galactic frame extends up to the escape velocity $\simeq 550 \text{ km/s}$. This is more than a factor of 2 larger than our speed relative to this frame, $v_{\text{sun}} \simeq 220 \text{ km/s}$. Inelastic dark matter, however, can scatter only once the dark matter speed is high enough in the lab frame to overcome the inelastic transition. For large inelastic transitions ($\delta \sim 300\text{-}600 \text{ keV}$), these high speeds can be obtained only by combining the high velocity tail of the galactic frame dark matter distribution with the boost into the Earth frame. Or, in other words, the very highest speeds of dark matter perceived in the Earth frame are unidirectional from the Cygnus constellation.

As δ is decreased from the maximum that permits any inelastic scattering, the range of speeds of dark matter which can scatter becomes larger. This also broadens the range of arrival directions from which dark matter can still inelastically scatter. We illustrate this in Fig. 2. The dark matter flux, when viewed as a distribution projected onto the sky in Earth frame (top panels), decreases rapidly away from the peak at Cygnus. Dark matter appearing from an increasingly larger region around Cygnus necessarily samples the increasingly suppressed dark matter velocity distribution tail.



DM speed distribution in Earth frame

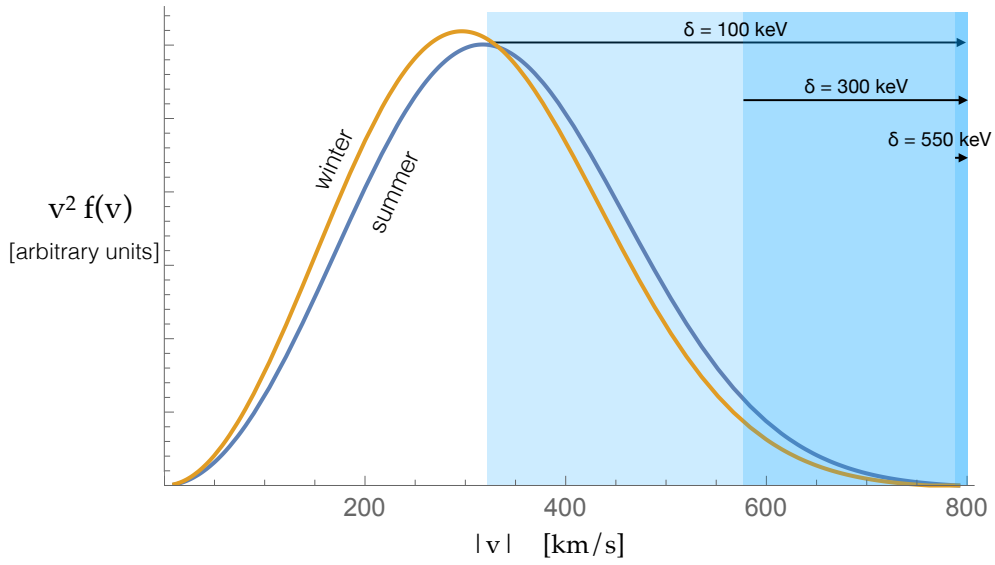


Figure 2: Upper four panels: The flux of 1 TeV dark matter capable of scattering off lead and its dependence on inelastic splitting, δ . The colors denote \log_{10} of the ratio of the flux to the peak flux, which comes from the direction of motion of the Earth, which is given by the cross and is approximately in the direction of the Cygnus constellation. Lower panel: The fraction of the velocity distribution of dark matter in the Earth frame that can scatter off lead for the same values of δ .

Unlike most other terrestrial beings that are interested in the position of the Sun, a dark matter direct detection experimenter ought to be interested in the position of Cygnus. Most dark matter particles, particularly those with high speed, appear to originate from the vicinity of Cygnus. This is obviously of importance if the detector has directional sensitivity [60]. Another example are models in which dark matter is sufficiently strongly interacting to have a high probability to scatter in the overburden. The rate in a detector will then depend on whether the line from the detector to Cygnus goes through ~ 1 km of rock above typical underground detectors or the entire diameter of the Earth (see e.g. [61]). In most “usual” weakly-coupled dark matter scenarios, by contrast, scattering off elements in the Earth occurs so rarely that the direction to Cygnus is irrelevant.

In our scenario, the overburden of the Earth is *critical* to obtaining a high signal rate. Dark matter inelastically scatters off material in the Earth, emerging as the excited state. As Fig. 2 shows, this implies the dark matter is most likely coming from the direction of Cygnus. During the hours that Cygnus is below the horizon the scattering may be, for example, in the Earth’s crust or mantle. The excited state travels a distance on average between ~ 10 –1000 km, then decays into the dark matter plus a photon with energy $E_\gamma = \delta$. When these decays occur inside an instrumented region, the photon can be detected. When Cygnus is above the horizon, there is a much smaller amount of overburden off which the dark matter can inelastically scatter, and a correspondingly smaller probability for the excited state to decay inside the detector since the detector depth is much smaller than the decay length. It is interesting that this is distinct from models with a very large scattering cross section, for which a large overburden leads to a substantially reduced rate [61]. In either case, the orientation of the detector relative to Cygnus is of paramount importance.

While the Sun returns to the same position in the sky every 24 hours – a solar day – the fixed stars return every *sidereal* day which is approximately 4 minutes shorter. Ignoring the very small shift (parallax) in the location of stars due to the Earth’s rotation around the Sun¹, all of the fixed stars (and constellations) rise and set at fixed sidereal times that are determined solely by the declination of the star in the Earth’s reference frame and the location on Earth.

Cygnus has a declination of approximately 45° North. This means detectors in the Northern Hemisphere at latitudes above 45° North see Cygnus above the horizon at all times of the sidereal day. Conversely, (hypothetical) detectors in the Southern Hemisphere below 45° South never see Cygnus above the horizon. In this paper we consider primarily three locations for detectors: Gran Sasso at 42.6° North (home to the Borexino experiment; also one of the locations for the CYGNUS directional dark matter experiment), Jiangmen at 22.1° North (where the JUNO experiment will be located), and SUPL at 37.1° South (where we consider a hypothetical Borexino-like experiment for the purposes of studying the unusual signals that could be seen in the Southern Hemisphere). In all of these cases, Cygnus is below the horizon for part of each sidereal day – about 2.5 hours for Gran Sasso, 8.5 hours for Jiangmen, and 18.5 hours for SUPL. The modulation of our signal will be determined by this sidereal schedule or the rise and set of Cygnus.

¹As well as the eccentricity of the Earth’s wobble that occurs on a much longer timescale than is relevant for dark matter direct detection.

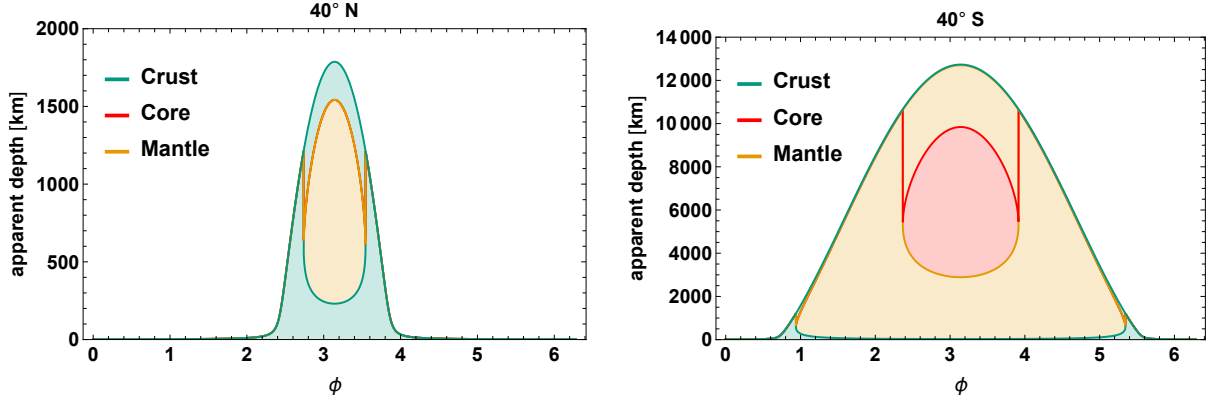


Figure 3: The distance through the Earth from a point 2 km below the Earth’s surface at 40° North (left) and South (right) of the equator, along the direction to Cygnus, through a (sidereal) day; $0 < \phi \leq 2\pi$.

3.2 Anisotropy of the overburden

Since our signal depends on the overburden which dark matter must traverse to reach a detector, it is worthwhile studying the overburden, including its anisotropy and elemental composition.

We can gain some insight into daily modulation effects by considering the apparent depth of a lab along the direction to Cygnus. The center of the Cygnus constellation is at about 45° declination, which is close to the latitude of Gran Sasso, see Tab. 2, meaning that the apparent depth of Gran Sasso is never particularly large. However, for a lab whose latitude lies below the declination of Cygnus, the depth becomes larger. We show in Fig. 3 the apparent depth for two underground labs, each at a depth of 2 km, at 40° North and South of the equator.

How much of the apparent depth is relevant to our signal depends on the lifetime of the excited state. As we saw from Eq. (3), typical decay lengths range from ~ 10 – 1000 km for $\delta \sim 550$ – 100 keV respectively, for dark matter with a mass of $m_1 = 1$ TeV. These lengths are fascinating, because they are significantly larger than the depth of underground detectors, but they may be considerably shorter than the Earth’s radius. As a result the signal rate depends on the composition of the Earth.

For heavier dark matter, $m_{\chi_1} \gtrsim m_{\text{nucleus}}$, and large inelastic splittings $\delta \gtrsim 150$ keV, the element with the largest probability to inelastically scatter off is lead. Lead is the most massive element in the Earth which is both relatively abundant and stable. Its abundance is roughly 10^{-5} g/g in the Earth’s crust [62] and a factor of five smaller in the mantle [63]. Moreover, lead (with $A \simeq 210$) is heavier than all of the elements used in direct detection experiments, providing a kinematic advantage for highly inelastic dark matter $\delta \gtrsim 350$ keV where there is no bound from other experiments. For lighter dark matter and/or lower splittings we will also consider scattering off of iron and silicon.

The details of the signal may also depend on geology, particularly on the difference between the crust and the mantle. In Fig. 3 we show separately the line of sight depth to Cygnus through

the core, crust and mantle. Which of these layers dominates the total rate will depend upon the lifetime of the excited state and the relative abundances of elements that dark matter can upscatter. The full analysis, below, takes all of this into account.

In most cases the effect of crust-mantle differences are small; however there are models in which it is important. A notable curious example is a model with $\delta \gtrsim 300$ keV and detectors in the southern hemisphere. In this case, the characteristic decay length is less than 100 km, and due to its higher lead abundance, the crust dominates over the mantle. As can be seen in the right panel of Fig. 3, the apparent depth of crust peaks at two separate angles $\phi \simeq \pi/3, 5\pi/3$, which will lead to a novel double-peaked modulation pattern which will be shown in detail in Sec. 3.5.

3.3 Anisotropic scattering

The third anisotropic effect which was implicitly assumed in the previous subsections, but is required in order to get a large modulation of our signal rate, is the angular distribution of the outgoing (excited-state) dark matter particles following a scattering off a nucleus in the Earth. In the center of mass frame, the scattering of dark matter off a nucleus is generically isotropic. However, if the dark matter is significantly heavier than the target nucleus, the center of mass frame and the lab frame are not coincident. As a result, for heavy dark matter the isotropic distribution is boosted and the dark matter scattering is mostly forward in the lab frame.

In the lab frame, the maximal deflection angle of the outgoing dark matter for the elastic dark matter case is

$$\cos \theta_{\max}^{\text{lab}} = \sqrt{1 - \frac{m_T^2}{m_{\chi_1}^2}}, \quad (6)$$

for a target mass m_T and a dark matter mass of m_{χ_1} . For dark matter of order a TeV, the dark matter is deflected at most $\sim 10^\circ$ off its original course, even if it scatters off a lead nucleus. We shall see in the next subsection that in the inelastic case this result is qualitatively unchanged, though Eq. (6) does receive a correction, see Eq. (12). The small deflection in the direction of the incoming dark matter, coupled with the anisotropic effects of the previous subsections, leads to a daily modulating event rate for heavy dark matter. In this work we will mostly focus on two target nuclei, iron and lead, and thus daily modulation is present for dark matter masses of a few hundred GeV or above. In Ref. [43], where dark matter is light in order to address DAMA, the daily modulation effect is not present for the dominant scattering off iron. It may be interesting to consider the sidereal-daily modulating signal for light dark matter scattering off lighter elements in the Earth or even off electrons, but this is left for future investigation.

3.4 Calculation of the modulating event rate

While useful intuition can be gained from studying the overburden as a function of lab location or assuming all dark matter comes from the direction of Cygnus (see Sec. 3.1), the full calculation must take into account the excited state's lifetime, the distribution of incoming dark matter velocities,

-	n_{Si} [km ⁻³]	n_{Fe} [km ⁻³]	n_{Pb} [km ⁻³]	Outer Radius [km]
Core	1.4×10^{37}	1.0×10^{38}	1.3×10^{31}	3483
Mantle	2.1×10^{37}	3.1×10^{36}	2.4×10^{30}	6341
Crust	1.7×10^{37}	2.0×10^{36}	8.4×10^{31}	6371

Table 1: Number densities for silicon, iron, and lead, along with the outer-edge radii, for the core [64], mantle [63], and crust [62, 65] in our three-layer approximation of the Earth.

the position of the detector, form factors, and the distribution of target elements within the Earth. We now present the details of the full calculation, which must be done numerically.

For a photon to be observed at an underground detector, an incoming dark matter particle must enter the Earth with sufficient speed that it can scatter off a target nucleus in the Earth at position \vec{r}_s , creating an excited state. This excited state must scatter through the appropriate angle, such that it then travels, with velocity \vec{v}_f , towards the detector, which is at \vec{r}_D , and it must decay between entering and leaving the detector. We take the scattering and the decay to be isotropic in their center of mass frames. The amount of available scattering material grows as $|\vec{r}_s - \vec{r}_D|^2$ but the probability to scatter towards the detector scales as $|\vec{r}_s - \vec{r}_D|^{-2}$. Thus, all scatter sites within a decay length of the detector are (approximately) equally important. Once the separation becomes larger than $v_f \tau$, decays become important. The interplay between scatter site, elemental abundances and lifetime is complicated.

The total rate is calculated by integrating over all possible scatter sites, \vec{r}_s , in the Earth. To model the distribution of target nuclei, we use a three-layer model of the Earth corresponding to the core, mantle, and crust. The number density $n_T(\vec{r}_s)$ of targets is a function of \vec{r}_s insofar as the density is different in the core [64], mantle [63], and crust [65]. We consider the cases where the target atoms are iron nuclei, lead nuclei, and to a lesser extent silicon nuclei; see Tab. 1. As might be imagined, determining the abundance of elements within the Earth is a challenging endeavor. By comparison to the chemical composition of chondritic meteorites, rocks from the upper mantle and core samples of the crust, one can infer an abundance of each element in the core, mantle and crust. The uncertainties on these numbers are at best 10 – 20%. Furthermore, these are average abundances and there are undoubtedly large local variations. We use only the central average value and do not attempt to incorporate uncertainties in abundances in our rate calculations.

As discussed earlier (see Sec. 3.1), for an upscatter to occur in the collision, the incoming dark matter must have high speed in the lab frame, which leads to a strong directionality in flux. In the galactic frame, the dark matter speed follows a Maxwell-Boltzmann distribution $f_{\text{gal}}(\vec{v}_{\text{MB}}) \propto \exp(-v_{\text{MB}}^2/v_0^2) \theta(v_{\text{esc}} - v_{\text{MB}})$, and we take $v_0 = 220$ km/s, $v_{\text{esc}} = 550 \pm 50$ km/s, the latter approximating the results from [66]. The total velocity of the dark matter relative to the Earth in galactic coordinates is

$$\vec{v}_\chi^{\text{gal}}(t) = \vec{v}_{\text{MB}} + \vec{v}_{\text{LSR}} + \vec{v}_{\text{pec}} + \vec{u}_E(t) . \quad (7)$$

This expression takes into account the velocity of the local standard of rest $\vec{v}_{\text{LSR}} = v_0 \hat{y}^{\text{gal}}$, the peculiar velocity of the Sun $\vec{v}_{\text{pec}} = (11.1, 12.2, 7.3)$ km/s, and the Earth’s velocity around the Sun $\vec{u}_E(t)$, which varies over a sidereal year. The combination of these velocities means that the dark

matter wind comes from $\sim 47^\circ$ declination, inside the Cygnus constellation. In determining the Earth's velocity around the Sun, we follow the procedure of Ref. [59]. Combining these relative motions gives the net velocity of dark matter relative to the Earth in the galactic coordinate system. However, one must also know the position of the scatter site and the lab in the same coordinate system as the velocity, which requires transforming between galacto-centric coordinates and Earth-centric (also called equatorial) coordinates. The two frames are related by a series of rotations, $R_i(\theta)$, through angle θ around axis i ,

$$\vec{v}_\chi^{\text{gal}} = R_y(\theta_\odot) \cdot R_x(\eta) \cdot R_z(\alpha_{\text{GC}}) \cdot R_y(\delta_{\text{GC}}) \cdot \vec{v}_\chi^{\text{equ}}. \quad (8)$$

Here, the right ascension of the galactic centre (GC) is $\alpha_{\text{GC}} = 266^\circ$, the declination is $\delta_{\text{GC}} = -29.0^\circ$, $\eta = 58.6^\circ$, and θ_\odot is determined by the height of the Sun above the galactic midplane, $\sin \theta_\odot = z_\odot/d_{\text{GC}}$. Of course, the magnitude of the velocity is unchanged under rotation and we denote the speed as v_χ .

Now that we have determined the incoming velocity in the lab frame, we turn to the kinematics of the initial scatter. Although we assume the scattering cross section is isotropic in the center of mass frame, the outgoing excited state will be forward, for the masses of dark matter we consider. The kinematics in the center of mass frame are straightforward and the outgoing speed in this frame is given by

$$v_{\text{out}}^{\text{cm}} = \left[\frac{\mu_2}{m_2} (\mu_1 v_\chi^2 - 2\delta) \right]^{1/2}, \quad (9)$$

with $\mu_{(1,2)} = m_{(1,2)} m_T / (m_{(1,2)} + m_T)$ the reduced mass of the target and the incoming and outgoing dark matter. The corresponding outgoing speed in the lab frame satisfies

$$v_{\text{out}}^{\text{lab}} = \left[(v_{\text{out}}^{\text{cm}})^2 + \left(\frac{\mu_1 v_\chi}{m_T} \right)^2 + \frac{2\mu_1 v_\chi v_{\text{out}}^{\text{cm}}}{m_T} \cos \theta^{\text{cm}} \right]^{1/2}. \quad (10)$$

The scattering angle in the lab frame is related to the scattering angle in the center of mass frame through

$$v_{\text{out}}^{\text{lab}} \cos \theta^{\text{lab}} = v_{\text{out}}^{\text{cm}} \cos \theta^{\text{cm}} + \frac{\mu_1 v_\chi}{m_T}. \quad (11)$$

This angle is limited kinematically, with a maximum value $\theta_{\text{max}}^{\text{lab}}$ which satisfies

$$\cos^2 \theta_{\text{max}}^{\text{lab}} = 1 - \left(\frac{m_T v_{\text{out}}^{\text{cm}}}{\mu_1 v_\chi} \right)^2 = \left(1 + \frac{m_T}{m_2} \right) \left(1 - \frac{m_T}{m_1} + \frac{2m_T \delta}{(m_1 v_\chi)^2} \right). \quad (12)$$

The minimum velocity (in the lab frame) required to upscatter is given by $v_{\text{min}} = \sqrt{2\delta/\mu_1}$; at large values of δ , v_{min} will exceed the largest allowed value of v_χ , driving the signal rate to zero.

The scattering angle necessary to reach the detector, θ^{lab} , must lie within the cone subtended by opening angle $\theta_{\text{max}}^{\text{lab}}$, and the fraction of the cone that the detector covers is given by $[R_D / (|\vec{r}_s - \vec{r}_D| \theta_{\text{max}}^{\text{lab}})]^2$, where R_D is the radius of the detector; for example, for Borexino $R_D = 5.5$ m (see Tab. 2). There are two possible center of mass frame scattering angles that will result in the excited dark matter arriving at the detector, leading (in the lab frame) to two different outgoing speeds for the excited dark matter,

$$v_{\text{out},\pm}^{\text{lab}} = \frac{m_1 v_\chi}{m_2 + m_T} \cos \theta^{\text{lab}} \left[1 \pm \sqrt{1 - \frac{\cos^2 \theta_{\text{max}}^{\text{lab}}}{\cos^2 \theta^{\text{lab}}}} \right]. \quad (13)$$

These two solutions take different lengths of time to get from the scatter site to the detector. The probability that an excited state moving at speed $v_{\text{out}}^{\text{lab}}$ will travel a distance $L = |\vec{r}_s - \vec{r}_D|$ and decay inside the detector is

$$P(v_{\text{out}}^{\text{lab}}, L, \tau) = 2 \sinh\left(\frac{R_D}{2 v_{\text{out}}^{\text{lab}} \tau}\right) \exp\left(-\frac{L}{v_{\text{out}}^{\text{lab}} \tau}\right). \quad (14)$$

Similarly, for the two possible center of mass scattering angles there are two different values of momentum exchanged with the nucleus, resulting in two different form factor suppressions. To account for the substructure of the nucleus, we use the Helm form factor [67]

$$F(q) = \frac{3}{q r_n} J_1(q r_n) \exp\left(-\frac{q^2 s^2}{2}\right), \quad (15)$$

with $s \approx 0.9$ fm and $r_n \approx 1.14 (A/0.93149)^{1/3}$ fm, and where $q = \sqrt{2 m_T E_R}$ is the momentum transfer in the collision.

In the center of mass frame the cross section is isotropic and almost independent of the incoming velocity,

$$\frac{d\sigma}{d \cos \theta^{\text{cm}}} = \sigma_0 \sqrt{1 - \frac{2\delta}{\mu_1 v_\chi^2}} \left(\frac{m_1}{m_1 + m_T}\right)^2 A^4, \quad (16)$$

where A the mass number of the target nucleus. To determine the fraction of scatters that end up in the detector, we must integrate over all scattering angles in the lab frame. The transformation to the lab frame introduces a Jacobian

$$J_{\pm}(v_\chi) = \frac{d \cos \theta^{\text{cm}}}{d \cos \theta^{\text{lab}}} = 2 z \cos \theta^{\text{lab}} \pm \frac{1 - z^2 + 2 z^2 \cos^2 \theta^{\text{lab}}}{\sqrt{1 - z^2 + z^2 \cos^2 \theta^{\text{lab}}}},$$

with $z = \mu_1 v_\chi / (m_T v_{\text{out}}^{\text{cm}})$.

Putting all these effects together we arrive at the final result for the expected rate inside the detector,

$$\Gamma = \sum_{\pm} \int d^3 r_s d^3 v_{\text{MB}} \left\{ n_T(r_s) \frac{\rho_\chi}{m_1} \left[\frac{R_D}{|\vec{r}_s - \vec{r}_D| \theta_{\text{max}}^{\text{lab}}} \right]^2 P(v_{\text{out}, \pm}^{\text{lab}}, L, \tau) \right. \\ \left. \times f_{\text{gal}}(v_{\text{MB}}) |F(q_{\pm})|^2 \frac{d\sigma v_\chi}{d \cos \theta^{\text{cm}}} |J_{\pm}(v_\chi)|^2 \right\}. \quad (17)$$

In the results presented below we have evaluated this integral numerically.

3.5 Results for modulating rates

We now present the results for the signal rate as a function of the time of day in a few representative experiments. We consider three different lab locations: Gran Sasso in Italy, Jiangmen in China, and SUPL in Australia. Gran Sasso is home to the Borexino detector [54] and is also one of the possible locations for CYGNUS [68, 69], a large gas TPC for directional dark matter detection. Jiangmen

Lab	Detector	latitude	longitude	depth [km]	Radius [m]
Gran Sasso	Borexino	42.7° N	13.6° E	1.4	5.5
Gran Sasso	CYGNUS	42.7° N	13.6° E	1.4	1-10
Jiangmen	JUNO	22.1° N	112.5° E	0.48	17
SUPL	hypothetical	37.1° S	143° E	1.0	5.5

Table 2: The position, depth, and size of various underground detectors, both existing and proposed, which are analyzed in this work. SUPL is the Stawell Underground Physics Laboratory in Australia, and we place a hypothetical Borexino-like detector there.

will host the JUNO neutrino detector [70], which will be notably larger than Borexino. We also consider a hypothetical Borexino-like detector at SUPL. The lab locations and detector sizes are shown in Tab. 2.

The rates calculated using Eq. (17) are shown in Fig. 4 for TeV dark matter with mass splittings of 150 and 500 keV for the three liquid scintillation detectors we consider. For the lifetime of the excited state, we use Eq. (3) for a higgsino (this assumption will be relaxed below).

The curves show the rate (in events/s) over a period of one day: the first day of March (red), June (blue), September (yellow), and December (purple). The first feature to notice is that the rate modulates strongly, as expected. Secondly, the time of day of the peak rate changes throughout the year. This is because the rate modulates with a period of a sidereal day, which is approximately four minutes shorter than the solar day. It is interesting to note that our modulation effect would be washed out if one were searching for a (solar) day-night asymmetry with an exposure of several years. These distinct modulation patterns can be used to discriminate signal from backgrounds, as we will show in the next section. The modulation patterns in Fig. 4 have some interesting characteristics:

- For high δ the rate modulates significantly both with a period of a sidereal day and annually. The later is due to the usual enhanced modulation of inelastic dark matter.
- In comparing the rate at Borexino and JUNO one can see that the peaks of an enhanced rate are wider in JUNO. This is because it is located further south, where Cygnus spends more of the day below the horizon.
- In all of the plots, we see the peak rate shifts by approximately 6 solar hours from season to season due to the difference between the solar and the sidereal day durations.
- In comparing the left and right in the top two panels of Fig. 4, we notice the the transition from high to low rate occurs more sharply for high δ as compared to low. This is because large splitting requires faster incoming dark matter. As shown in the top of Fig. 2, the dark matter particles are coming from a more focused region in the sky. The smaller spot takes less time to set below the horizon leading to a faster transition.
- In the Southern Hemisphere, the Cygnus constellation does not rise far above the horizon, as a result, the rate at SUPL does not drop as close to zero as compared to the Northern Hemisphere detectors.

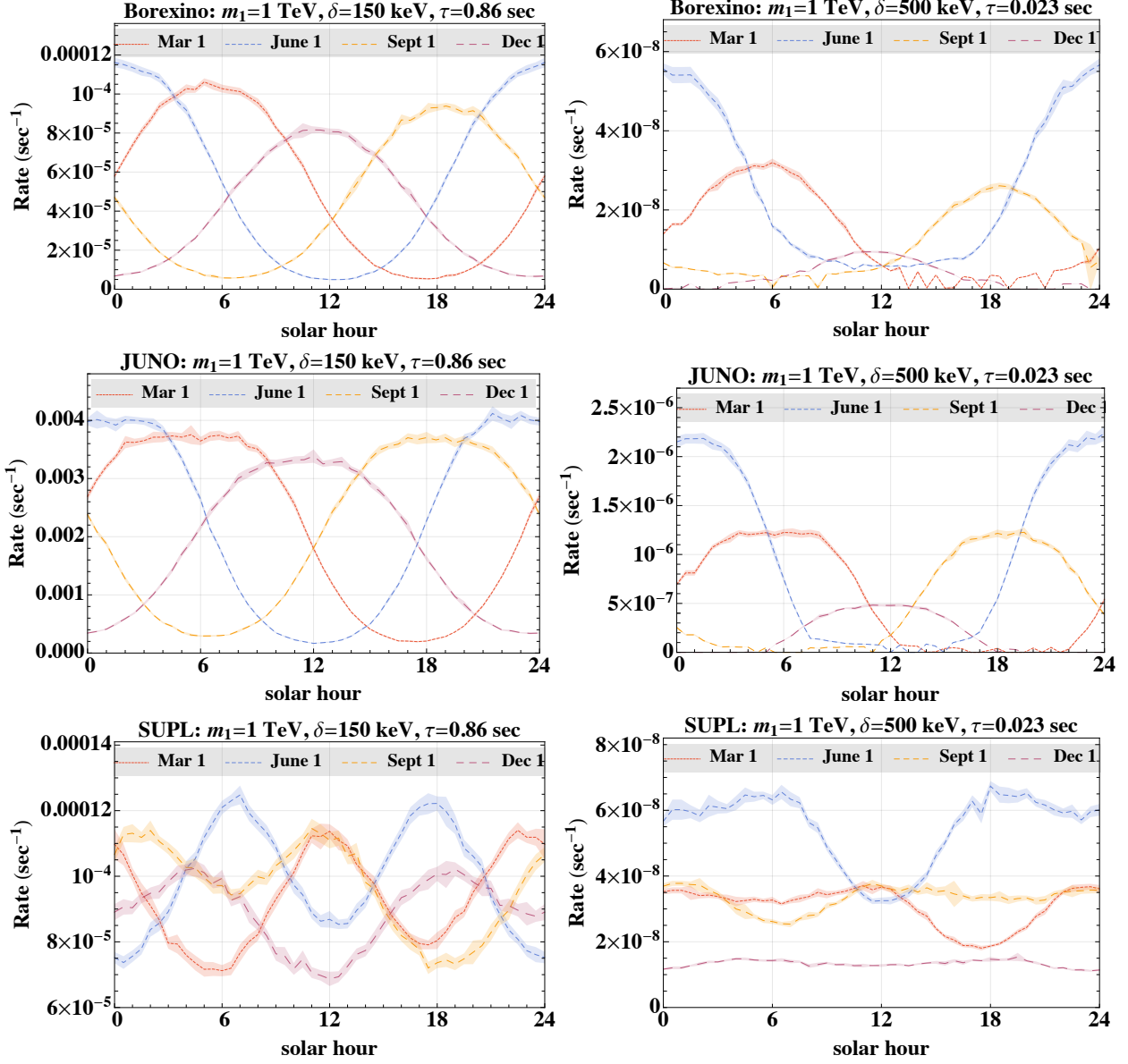


Figure 4: The expected signal rates for the Borexino detector (top row), JUNO detector (middle row), and a hypothetical detector at SUPL (bottom row). The curves show the rate over one solar day: the first day of March (red), June (blue), September (yellow), and December (purple). The rate was determined using Eq. (17) with $m_\chi = 1$ TeV and lifetime given by the decay length of Eq. (3); the mass splitting in the left (right) panels is $\delta = 150$ (500) keV. The results are shown in a common time-zone for all labs for ease of comparison.

- Notice that there are some interesting doubly-peaked modulation patterns in the Southern Hemisphere. These can be understood by noticing that the Earth's crust is richer in lead, than is the mantle. Inspecting Fig. 3 one sees that the crust contribution to the apparent

depth peaks at two distinct times during the sidereal day: once when Cygnus sets and once when it rises.

- While the event rate per day can be very small, a modulating signal can be seen above background by stacking across multiple days. This requires a long exposure of the experiment and/or a larger signal cross section, as we will show in Sec. 4.

The fact that the signal modulates is expected to be quite robust to changes in the lifetime of the excited state χ_2 , although the quantitative details will vary with lifetime. This is because, as the lifetime grows, the effective volume for scattering that can reach the detector grows, while the angular acceptance of the added volume is correspondingly smaller. However, as the lifetime of the excited state grows, different parts of the Earth contribute. In addition, if the lifetime exceeds the crossing time of the Earth, the signal rate begins to decrease linearly as $v\tau/R_\oplus$. To demonstrate this, in Fig. 5 we plot the modulation rate in several detectors for varying χ_2 lifetimes. The linear drop in event rate is seen clearly. In addition, the differences in shape between lifetimes of 0.36 seconds and longer lifetimes is because the former is sensitive to the Earth composition closer to the detector whereas longer lifetimes probe the whole Earth. For example, the double peak structure in the Southern Hemisphere disappears when the whole Earth is probed.

4 Current and Future Sensitivities

We are now ready to estimate the sensitivity of modulating luminous signals to inelastic dark matter. We will focus on two regions of parameter space which can be probed by two different types of detectors. In Sec. 4.1, we consider higher mass splitting, $\delta \gtrsim 200$ keV, which can be probed by detectors with a high threshold, such as the large liquid scintillator neutrino detectors Borexino and JUNO. In Sec. 4.2, we will consider low mass splittings which can be probed by large gaseous detectors designed for dark matter directional detection, such as the proposed CYGNUS detector.

4.1 Sensitivity of Borexino and JUNO

In this section, we consider the Borexino detector and events observed during its running of 1291.5 days [54]. The observed rate in the vicinity of 250-600 keV is 0.1–0.5 events/(day×keV×100 tonnes). This rate does not include the radioactive background from ^{210}Po α -decay, since it can be effectively subtracted using a fit of shower shape variables (see e.g. Figure 53 of [54]). The rate is dominated by the ^7Be neutrino signal, which amusingly serves as a background for our analysis. There are also several radioactive backgrounds which play a significant role. Below 250 keV the ^{14}C background dominates, producing a much higher background rate. The background rate that we use to place our bounds is shown in Fig. 6, and was extracted from [71] and [54]. In our estimate we will *not* assume any fundamental understanding of these backgrounds but will instead make use of the daily modulation of the signal.

The luminous dark matter signal is a spectral line at an energy $E_\gamma \simeq \delta$ on top of this background. This line is smeared by the energy resolution which we take to be $\sim 10\%$ [54]. The

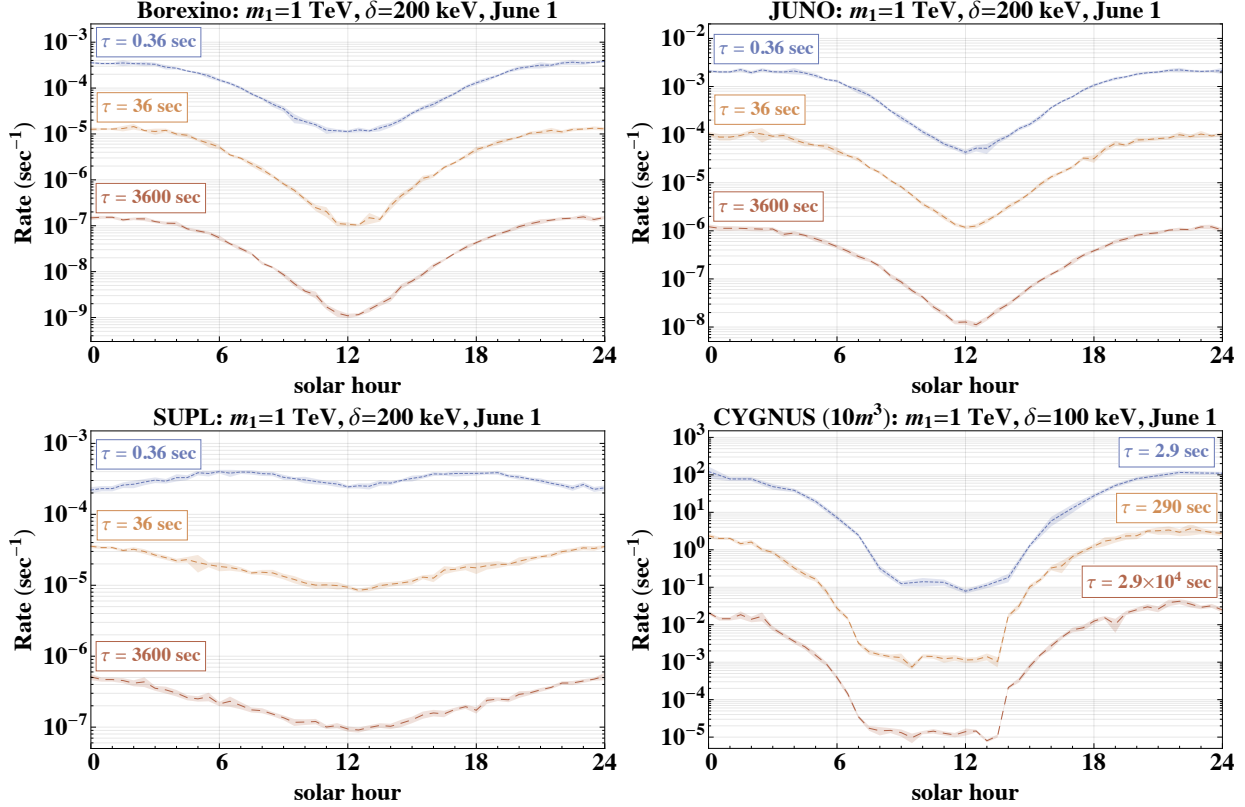


Figure 5: The total signal rate at $\delta = 200$ keV over one day for Borexino (top left), JUNO (top right), and SUPL (bottom left), and the rate for $\delta = 100$ keV for a 10m^3 CYGNUS-like detector (bottom right); the lifetime is taken to be $\tau = \ell_{\chi_2}/c$ (blue), $10^2\ell_{\chi_2}/c$ (yellow), and $10^4\ell_{\chi_2}/c$ (red), where ℓ_{χ_2} is given by Eq. (3).

background rate within the line width is thus of order 5 events per day in Borexino for photon energies above 250 keV. If it were not for the daily modulation of the signal, a conservative bound would require that the luminous photon signal rate be below the observed background rate. This would not make use of the large exposure of Borexino. However, the limit obtained by a modulation analysis is much stronger and does take advantage of the order thousand tonnes \times year exposure of Borexino.

Performing a full-fledged modulation analysis is beyond the scope of our work. We instead follow a simpler (though cruder) approach – dividing the sidereal day into two bins: signal-“on” and signal-“off”. For simplicity we take each bin to be one-half of a sidereal day. The “on” bin consists of the half-day in which the integrated signal rate is maximal, while the “off” bin is the other half-day in which the signal rate is lowest. In most of the parameter space of interest, the signal rate during the on bin will be much larger than that in the off bin, $\Gamma_s^{\text{on}} \gg \Gamma_s^{\text{off}}$ and the off rate can be neglected². In the Northern Hemisphere the on bin consists of twelve consecutive sidereal hours, but this does not have to be the case in general as can be seen in Fig. 4.

²In the off bin the signal is not quite off, but the validity of this approximation justifies its name.

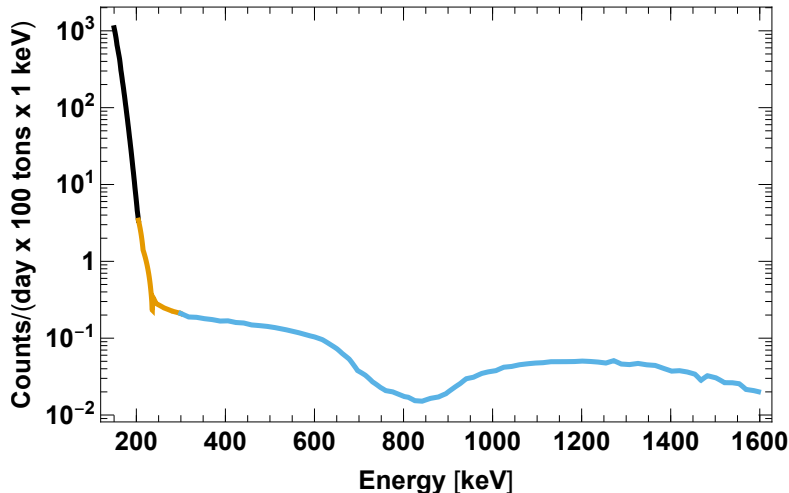


Figure 6: The background rate at Borexino. The black curve is extracted from [71] while the orange and blue curves come from [54].

Employing this on-off approximation, one can “measure” the backgrounds using the signal-off bin and use this to help search for the signal in the signal-on bin. The uncertainty in the prediction of the background in the on bin will thus be set by the statistical uncertainty of the measurement in the off bin. Suppose that during Borexino’s full run it has accumulated N_{off} events during signal-off times in a window of size $\pm 0.1\delta$ around a hypothesized δ . The reach of Borexino can be estimated by requiring that the signal rate in the signal-on bin, Γ_{signal} , does not exceed the expected statistical fluctuations in the background rate in the signal-off bin,

$$\Gamma_{\text{signal}} \lesssim \frac{2 \times 1.64}{\sqrt{N_{\text{off}}}} \Gamma_{\text{off}} \quad (18)$$

where $N_{\text{off}} = \Gamma_{\text{off}} t_{\text{off}}$ and $t_{\text{off}} = 1/2 \times 1291.5$ days is the total signal-off time accumulated in the exposure, and the factor of 1.64 arises because we consider a 90% confidence interval. This procedure yields an expected limit which strengthens as the square root of the exposure.

In Fig. 7 we show the sensitivity of Borexino for a 1 TeV higgsino with decay length determined by Eq. (3). This figure is one of the main results of this paper. The figure demonstrates that Borexino (and, in the future, JUNO) has the potential to substantially extend the bound on narrowly-split higgsinos, $\delta \gtrsim 380$ keV ($\delta \gtrsim 500$ keV), using an alternative search strategy to direct detection experiments. The weakening of the bound for $\delta \lesssim 250$ keV is due to the growth of the background at low energies, specifically ^{14}C . We expect that an actual analysis, using the time-stamps in the real data, will be able to improve upon our analysis at high δ and potentially look underneath this background which will not have a sidereal modulation.

The current bounds, also shown in Fig. 7, from the non-observation of nuclear recoil from inelastic scattering are derived from [14] and shown using the latest results from CRESST-II [72], PICO-60 [73], and XENON100 [23]. CRESST has accumulated 52 kg \times days of data with nuclear recoil energies between 20-120 keV_{nr}, they observed 4 events. PICO’s data corresponds to

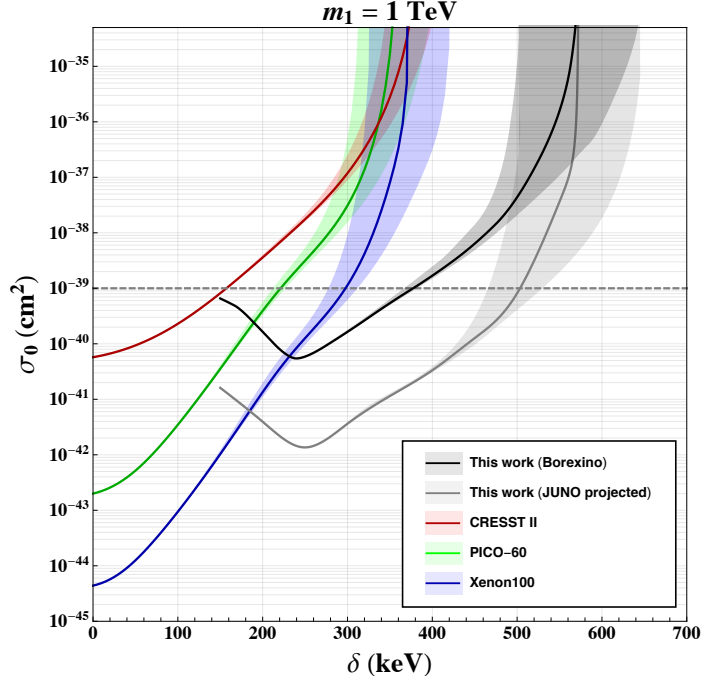


Figure 7: Projected sensitivity to the inelastic dark matter cross section in neutrino detectors. The red, green, and blue curves represent (respectively) existing direct detection bounds from CRESST II, PICO-60, and XENON100 (see [14]). The shaded regions of each curve represent the uncertainty in $v_{\text{esc}} = 550 \pm 50$ km/s. The black (gray) curves represent projected Borexino sensitivity using the existing 1291.5 days of running (projected JUNO sensitivity assuming Borexino-like background and run time). The dashed horizontal gray line is the scattering cross section for a narrowly-split higgsino.

~ 1300 kg \times days of exposure with a sensitivity to recoils between $10 - 10^3$ keV, the lower threshold varied over their data taking from 7 – 20 keV but we take the lower limit fixed at 10 keV, they did not observe any events. The conventional analysis of XENON100 [74] is over an energy range of 6.6-43.3 keV_{nr}. However, the collaboration have also carried out an analysis up to 240 keV_{nr}, corresponding to 3 – 180 PE in S1, and have presented their ~ 7600 kg \times days of data over an enlarged energy range, up to 1000 PE in S1 (see Figure 9 of Ref. [23]). They have not carried out a complete analysis over this full range, so the efficiencies for nuclear recoils are not known; we assume they are similar to those below 180 PE. Since they have not seen any events up to 1000 PE (~ 500 keV_{nr}), we place a bound. In all cases, after accounting for the mass fraction of the experiment made of the heavy target element, we must apply a rescaling to account for efficiency effects. We determine this rescaling by matching with the known constraint at $\delta = 0$ keV.

The sensitivity to the photon signal in Borexino (and presumably JUNO, in the future) is limited by radioactive backgrounds and solar neutrinos scattering off the elements in the liquid scintillator. The neutrino scattering was, after all, the motivation for the design of these experiments. Substantial improvement could be achieved if these “backgrounds” could be reduced. A similar sized detector but with a significantly reduced mass inside the detector, achieved by swap-

ping the liquid scintillator with a gaseous scintillator, would yield significant improvements in the sensitivity to luminous dark matter. In the regime $\delta \gtrsim 150$ keV, a Borexino-sized detector would see nearly two orders of magnitude improvement in the sensitivity to the luminous dark matter signal. Actually modifying the Borexino detector to use a gaseous scintillator would be very interesting, but undoubtedly is accompanied by numerous experimental challenges. However, as we see in the next section, directional dark matter detectors employ large volumes of gaseous scintillator that are ideal to reach sensitivity to a lower range of δ .

4.2 Sensitivity of gaseous scintillation detectors: CYGNUS

The rate of the photon signal from decay of the excited state scales with the *volume* of the detector and not the *mass* of the scintillation material. Since the backgrounds to the luminous signal scale with mass, the simplest way to reduce, and potentially eliminate, the backgrounds would be to change the detection technology from a liquid scintillator to a gaseous scintillator material.

Existing and proposed directional dark matter detectors including DMTPC [75], DRIFT [76] and CYGNUS [68, 69] employ a gaseous scintillation material. The sensitivity of these detectors to ordinary elastic dark matter scattering is limited by the mass of the scintillator, which is why they have primarily focused on gaseous elements sensitive to spin-dependent elastic scattering. The luminous dark matter signal, however, does not depend on scattering within the detector volume and is thus independent of the particular gas used. The luminous signal only requires good efficiency in converting the $\mathcal{O}(10 - 500)$ keV photon into scintillation light.

One of the principal benefits of the gaseous scintillator detectors is their low detection threshold for electromagnetic-equivalent energy deposition, of order few to 10 keV_{ee}, which is considerably lower than the threshold for neutrino detectors. In addition, some of the choices for the scintillation gas do not involve carbon (instead, SF₆ or He), which should decrease the radioactive background from ¹⁴C. Hence, gaseous scintillators can be sensitive to much lower energy photons coming from small mass differences, $\delta \gtrsim$ few to 10 keV, between the excited state and the dark matter.

Lower δ means lighter and more abundant elements in the Earth can be used to upscatter. While there are many elements lighter than lead that could be used to scatter, in the following we illustrate the sensitivity of the CYGNUS detector using upscattering off iron and silicon (as well as lead). Iron is the fourth most abundant element by mass in the Earth and has a number density that is 10⁵-10⁷ times larger than lead. Silicon is the second most abundant and has a number density a further 10 times larger than iron in the crust and the mantle (but 10 times smaller in the core), see Tab. 1. Upscattering is kinematically possible off iron with $\delta \lesssim 160$ keV and possible off silicon for $\delta \lesssim 85$ keV, which means gaseous detectors can probe a complementary range of inelastic parameter space.

In Fig. 8, we show the sensitivity that the CYGNUS detector, assumed to be sensitive to photon energies $5 \text{ keV} \leq E_\gamma \leq 200 \text{ keV}$, would be capable of reaching with several potential volumes (1, 10, and 1000 m³) after one year of exposure. Since these detectors have yet to be built, the background rate is not yet known. Estimates for a 10 m³ detector in the 1-10 keV_{ee} energy range have been presented in [68]. We extrapolated these estimates above the 1-10 keV_{ee} energy window, assuming

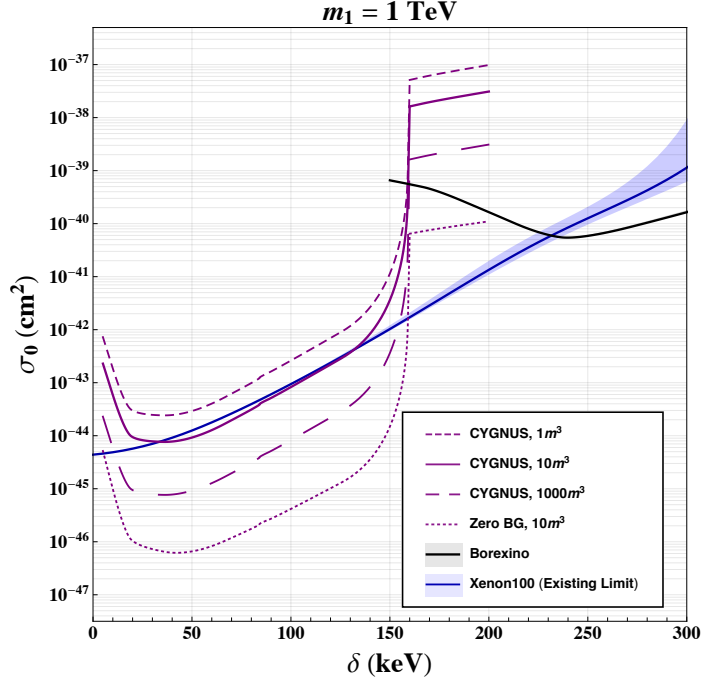


Figure 8: Projected sensitivity to the inelastic dark matter cross section in gaseous dark matter detectors such as CYGNUS. The blue curve represents existing direct detection bounds from XENON100, and the black solid line is the projected limit from Borexino, as in Fig. 7. The purple lines represent an experiment with CYGNUS-like background projections, with detector volume 1 m^3 (short dashed), 10 m^3 (thick), and 1000 m^3 (long dashed). The dotted purple line represents the projected sensitivity of a hypothetical zero-background experiment with detector volume 10 m^3 . For the CYGNUS curves, we only show the sensitivities with $v_{\text{esc}} = 550 \text{ km/s}$.

they are independent of energy, up to 200 keV and also assumed the background rates scale with detector volume for the larger possible detectors. We do not estimate the sensitivity for $\delta > 200$ keV since this is typically the highest energy at which existing directional detector collaborations have calibrated their detector response.

The dramatic increase in sensitivity below 160 keV is a result of inelastic dark matter being able to scatter off iron. In practice, there would be improved sensitivity even between $150 \text{ keV} \lesssim \delta \lesssim 200 \text{ keV}$ due to elements in the Earth that are more abundant than lead but also heavier than iron (such as barium). For $\delta \lesssim 85 \text{ keV}$ it is possible for dark matter to scatter off silicon, and for lower δ this will dominate. Once $\delta \lesssim 40 \text{ keV}$, the characteristic decay length, Eq. (3), exceeds the diameter of the Earth and the sensitivity decreases rapidly. Remarkably, a 10 m^3 detector employed to search for the luminous signal (and with a conservative assumption of the background as described above) has comparable sensitivity to what XENON100 has achieved by searching for the signal of inelastic nuclear recoil.

Larger volumes and/or lower backgrounds would significantly improve the sensitivity of CYGNUS to the luminous signal, see Fig. 8. CYGNUS is designed as a directional dark mat-

ter detector and will suppress backgrounds by using pointing of the dark matter recoil signal. The signal of luminous dark matter is not pointing but is instead modulating in a unique way. As discussed for Borexino this feature also allows good suppression of backgrounds. Since CYGNUS detector development is still underway, there are opportunities in design and material choices that are likely to reduce the background estimates. As an indication of the maximal possible reach we also show the sensitivity of a hypothetical CYGNUS-like 10 m^3 gaseous detector with zero background. The improvement in the sensitivity – over 100 times better – is highly significant since it would allow the CYGNUS detector to achieve *much* stronger sensitivity to inelastic dark matter with mass splittings up to about 150 keV.

5 Discussion

We demonstrated that we can use the Earth to inelastically upscatter dark matter into an excited state that later decays into a photon, providing an outstanding opportunity for dark matter detection. As shown in Figures 7 and 8, large underground experiments including both large neutrino experiments such as Borexino and JUNO as well as large directional detection experiments such as CYGNUS can achieve sensitivities to the photon decay signal that are significantly stronger than inelastically scattering off xenon in a conventional direct detection experiment. The improved sensitivities benefit greatly from the large sidereal-daily modulation that provides an excellent handle to separate signal from background. Both trace abundance of heavy elements like lead as well as the much more numerous elements such as iron and silicon provide the main scattering nuclei. This allowed us to obtain good estimates of the sensitivity of this technique, although we are still sensitive to uncertainties in the elemental abundances. More elements could be included in calculating the sensitivities, and a more nuanced model of their distribution in the Earth, but these would not qualitatively change our conclusions. For instance, we estimate that including the heaviest 20 elements in the Earth improves our sensitivity by less than a factor of 2. We emphasize that we have calculated Borexino’s expected sensitivity, and not a limit. Indeed, we encourage Borexino to re-analyze their data to look for a sidereal-daily modulating signal, as they could undoubtedly improve upon the crude statistical measures that we employed to obtain our estimates.

We also found that large gaseous scintillation detectors such as CYGNUS are sensitive to the photon decay signal with smaller inelastic splittings, $\delta \lesssim 160 \text{ keV}$, due to their lower detection threshold and the absence of a ^{14}C radioactive background. In fact, CYGNUS could be more sensitive to the photon signal at these lower inelastic splittings than the limits from inelastic nuclear recoil in existing xenon experiments.

In this paper our main focus was on dark matter that inelastically upscattered through one process (that could be due to Z -exchange) and decayed via a radiative decay. The notion that the upscatter process $\chi_1 + N \rightarrow \chi_2 + N$ is separate from the decay $\chi_2 \rightarrow \chi_1 + \gamma$ occurs generically in a wide variety of models, including narrowly-split higgsinos of split Dirac supersymmetry. In the narrowly-split higgsino model, the ordinary elastic scattering process does occur at one-loop, but is highly suppressed by the twist-2 suppression of the operator as well as an accidental cancellation among the diagrams.

It is also possible that the inelastic scattering process and the radiative decay proceed through the same operator. Magnetic inelastic dark matter [13, 20] is a known example of this. Derived bounds [14] on the magnetic inelastic interaction from XENON100 and PICO data require the characteristic decay length of the excited state be at least $\ell \gtrsim 10, 100, 1000$ m for $\delta \lesssim 150, 100, 50$ keV. The dark matter nucleus scattering in magnetic inelastic models involves several operators (in the notation of [13]). It was shown in [14] that for lower δ , the spin-independent interaction dominates, while for larger δ , the spin-dependent interaction dominates. This means that to determine the sensitivity of CYGNUS to magnetic inelastic dark matter requires a careful treatment of the Earth’s abundances of not only massive elements but also ones with a high spin. We will present this analysis in future work [77].

It is interesting to consider if other detectors could be sensitive to inelastic dark matter, possibly in other ranges of inelastic splittings. SNO+ [78] could be sensitive to a similar region of parameter space that we have presented for Borexino and JUNO. We did not calculate the sensitivity of SNO+ due to its latitude (most of the Cygnus constellation is always above the horizon at Sudbury) and its energy threshold being between 200-400 keV. It is an accident of circumstance (where deep mining for nickel in Canada happens to be located) that suggests SNO+ would have significantly poorer sensitivity compared to JUNO, where in its location much higher rates are expected. DUNE [79] also provides an interesting possibility for a large underground experiment that could be sensitive to a photon signal. Unfortunately, its threshold is higher than an MeV, and so it does not appear to be useful for galactic dark matter whose maximum speed is limited by the escape velocity of the galaxy. It is clear that the luminous signal of inelastic dark matter provides an additional, and orthogonal, search technique with which to hunt for dark matter. This “photon phrontier” may provide reach beyond that of the cross section or inelastic frontiers.

Acknowledgments

We thank M. Pospelov for being M. Pospelov (pointing out relevant physics in obscure sources). We thank R. Lang and N. Spooner for helpful discussion, and important information on XENON100 and CYGNUS, respectively. GDK thanks the Universities Research Association for travel support, and Fermilab for hospitality, where part of this work was completed. The work of JE was supported by the Zuckerman STEM Leadership Program. The work of PJF and RH was supported by the DoE under contract number DE-SC0007859 and Fermilab, operated by Fermi Research Alliance, LLC under contract number DE-AC02-07CH11359 with the United States Department of Energy. The work of GDK was supported in part by the U.S. Department of Energy under Grant Number DE-SC0011640.

References

- [1] L. J. Hall, T. Moroi, and H. Murayama, “Sneutrino cold dark matter with lepton number violation,” *Phys. Lett.* **B424** (1998) 305–312, [arXiv:hep-ph/9712515](#) [[hep-ph](#)].

- [2] D. Tucker-Smith and N. Weiner, “Inelastic dark matter,” *Phys. Rev.* **D64** (2001) 043502, [arXiv:hep-ph/0101138](#) [hep-ph].
- [3] D. Tucker-Smith and N. Weiner, “The Status of inelastic dark matter,” *Phys. Rev.* **D72** (2005) 063509, [arXiv:hep-ph/0402065](#) [hep-ph].
- [4] D. P. Finkbeiner and N. Weiner, “Exciting Dark Matter and the INTEGRAL/SPI 511 keV signal,” *Phys. Rev.* **D76** (2007) 083519, [arXiv:astro-ph/0702587](#) [astro-ph].
- [5] C. Arina and N. Fornengo, “Sneutrino cold dark matter, a new analysis: Relic abundance and detection rates,” *JHEP* **11** (2007) 029, [arXiv:0709.4477](#) [hep-ph].
- [6] S. Chang, G. D. Kribs, D. Tucker-Smith, and N. Weiner, “Inelastic Dark Matter in Light of DAMA/LIBRA,” *Phys. Rev.* **D79** (2009) 043513, [arXiv:0807.2250](#) [hep-ph].
- [7] Y. Cui, D. E. Morrissey, D. Poland, and L. Randall, “Candidates for Inelastic Dark Matter,” *JHEP* **05** (2009) 076, [arXiv:0901.0557](#) [hep-ph].
- [8] P. J. Fox, G. D. Kribs, and T. M. P. Tait, “Interpreting Dark Matter Direct Detection Independently of the Local Velocity and Density Distribution,” *Phys. Rev.* **D83** (2011) 034007, [arXiv:1011.1910](#) [hep-ph].
- [9] T. Lin and D. P. Finkbeiner, “Magnetic Inelastic Dark Matter: Directional Signals Without a Directional Detector,” *Phys. Rev.* **D83** (2011) 083510, [arXiv:1011.3052](#) [astro-ph.CO].
- [10] H. An, P. S. B. Dev, Y. Cai, and R. N. Mohapatra, “Sneutrino Dark Matter in Gauged Inverse Seesaw Models for Neutrinos,” *Phys. Rev. Lett.* **108** (2012) 081806, [arXiv:1110.1366](#) [hep-ph].
- [11] M. Pospelov, N. Weiner, and I. Yavin, “Dark matter detection in two easy steps,” *Phys. Rev.* **D89** (2014) no. 5, 055008, [arXiv:1312.1363](#) [hep-ph].
- [12] K. R. Dienes, J. Kumar, B. Thomas, and D. Yaylali, “Dark-Matter Decay as a Complementary Probe of Multicomponent Dark Sectors,” *Phys. Rev. Lett.* **114** (2015) no. 5, 051301, [arXiv:1406.4868](#) [hep-ph].
- [13] G. Barello, S. Chang, and C. A. Newby, “A Model Independent Approach to Inelastic Dark Matter Scattering,” *Phys. Rev.* **D90** (2014) no. 9, 094027, [arXiv:1409.0536](#) [hep-ph].
- [14] J. Bramante, P. J. Fox, G. D. Kribs, and A. Martin, “Inelastic frontier: Discovering dark matter at high recoil energy,” *Phys. Rev.* **D94** (2016) no. 11, 115026, [arXiv:1608.02662](#) [hep-ph].
- [15] C. Cheung, J. T. Ruderman, L.-T. Wang, and I. Yavin, “Kinetic Mixing as the Origin of Light Dark Scales,” *Phys. Rev.* **D80** (2009) 035008, [arXiv:0902.3246](#) [hep-ph].
- [16] P. W. Graham, R. Harnik, S. Rajendran, and P. Saraswat, “Exothermic Dark Matter,” *Phys. Rev.* **D82** (2010) 063512, [arXiv:1004.0937](#) [hep-ph].
- [17] N. Arkani-Hamed, D. P. Finkbeiner, T. R. Slatyer, and N. Weiner, “A Theory of Dark Matter,” *Phys. Rev.* **D79** (2009) 015014, [arXiv:0810.0713](#) [hep-ph].

- [18] D. S. M. Alves, S. R. Behbahani, P. Schuster, and J. G. Wacker, “Composite Inelastic Dark Matter,” *Phys. Lett.* **B692** (2010) 323–326, [arXiv:0903.3945 \[hep-ph\]](#).
- [19] M. Lisanti and J. G. Wacker, “Parity Violation in Composite Inelastic Dark Matter Models,” *Phys. Rev.* **D82** (2010) 055023, [arXiv:0911.4483 \[hep-ph\]](#).
- [20] S. Chang, N. Weiner, and I. Yavin, “Magnetic Inelastic Dark Matter,” *Phys. Rev.* **D82** (2010) 125011, [arXiv:1007.4200 \[hep-ph\]](#).
- [21] T. Schwetz and J. Zupan, “Dark Matter attempts for CoGeNT and DAMA,” *JCAP* **1108** (2011) 008, [arXiv:1106.6241 \[hep-ph\]](#).
- [22] N. Weiner and I. Yavin, “UV completions of magnetic inelastic and Rayleigh dark matter for the Fermi Line(s),” *Phys. Rev.* **D87** (2013) no. 2, 023523, [arXiv:1209.1093 \[hep-ph\]](#).
- [23] **XENON** Collaboration, E. Aprile *et al.*, “Effective field theory search for high-energy nuclear recoils using the XENON100 dark matter detector,” *Phys. Rev.* **D96** (2017) no. 4, 042004, [arXiv:1705.02614 \[astro-ph.CO\]](#).
- [24] **PandaX-II** Collaboration, X. Chen *et al.*, “Exploring the dark matter inelastic frontier with 79.6 days of PandaX-II data,” *Phys. Rev.* **D96** (2017) no. 10, 102007, [arXiv:1708.05825 \[hep-ex\]](#).
- [25] H. Davoudiasl, D. E. Morrissey, K. Sigurdson, and S. Tulin, “Hylogenesis: A Unified Origin for Baryonic Visible Matter and Antibaryonic Dark Matter,” *Phys. Rev. Lett.* **105** (2010) 211304, [arXiv:1008.2399 \[hep-ph\]](#).
- [26] H. Davoudiasl, D. E. Morrissey, K. Sigurdson, and S. Tulin, “Baryon Destruction by Asymmetric Dark Matter,” *Phys. Rev.* **D84** (2011) 096008, [arXiv:1106.4320 \[hep-ph\]](#).
- [27] H. An, M. Pospelov, and J. Pradler, “Direct constraints on charged excitations of dark matter,” *Phys. Rev. Lett.* **109** (2012) 251302, [arXiv:1209.6358 \[hep-ph\]](#).
- [28] J. Huang and Y. Zhao, “Dark Matter Induced Nucleon Decay: Model and Signatures,” *JHEP* **02** (2014) 077, [arXiv:1312.0011 \[hep-ph\]](#).
- [29] H. Yuksel, S. Horiuchi, J. F. Beacom, and S. Ando, “Neutrino Constraints on the Dark Matter Total Annihilation Cross Section,” *Phys. Rev.* **D76** (2007) 123506, [arXiv:0707.0196 \[astro-ph\]](#).
- [30] K. Agashe, Y. Cui, L. Necib, and J. Thaler, “(In)direct Detection of Boosted Dark Matter,” *JCAP* **1410** (2014) no. 10, 062, [arXiv:1405.7370 \[hep-ph\]](#).
- [31] J. Berger, Y. Cui, and Y. Zhao, “Detecting Boosted Dark Matter from the Sun with Large Volume Neutrino Detectors,” *JCAP* **1502** (2015) no. 02, 005, [arXiv:1410.2246 \[hep-ph\]](#).
- [32] K. Kong, G. Mohlabeng, and J.-C. Park, “Boosted dark matter signals uplifted with self-interaction,” *Phys. Lett.* **B743** (2015) 256–266, [arXiv:1411.6632 \[hep-ph\]](#).
- [33] H. Alhazmi, K. Kong, G. Mohlabeng, and J.-C. Park, “Boosted Dark Matter at the Deep Underground Neutrino Experiment,” *JHEP* **04** (2017) 158, [arXiv:1611.09866 \[hep-ph\]](#).

- [34] Y. Cui, M. Pospelov, and J. Pradler, “Signatures of Dark Radiation in Neutrino and Dark Matter Detectors,” *Phys. Rev.* **D97** (2018) no. 10, 103004, [arXiv:1711.04531 \[hep-ph\]](#).
- [35] **Super-Kamiokande** Collaboration, C. Kachulis *et al.*, “Search for Boosted Dark Matter Interacting With Electrons in Super-Kamiokande,” *Phys. Rev. Lett.* **120** (2018) no. 22, 221301, [arXiv:1711.05278 \[hep-ex\]](#).
- [36] A. Olivares-Del Campo, C. Boehm, S. Palomares-Ruiz, and S. Pascoli, “Dark matter-neutrino interactions through the lens of their cosmological implications,” *Phys. Rev.* **D97** (2018) no. 7, 075039, [arXiv:1711.05283 \[hep-ph\]](#).
- [37] D. Kim, K. Kong, J.-C. Park, and S. Shin, “Boosted Dark Matter Quarrying at Surface Neutrino Detectors,” *JHEP* **08** (2018) 155, [arXiv:1804.07302 \[hep-ph\]](#).
- [38] D. McKeen and N. Raj, “Monochromatic dark neutrinos and boosted dark matter in noble liquid direct detection,” [arXiv:1812.05102 \[hep-ph\]](#).
- [39] J. Bramante, B. Broerman, J. Kumar, R. F. Lang, M. Pospelov, and N. Raj, “Foraging for dark matter in large volume liquid scintillator neutrino detectors with multiscatter events,” [arXiv:1812.09325 \[hep-ph\]](#).
- [40] Y. Grossman, R. Harnik, O. Telem, and Y. Zhang, “Self-Destructing Dark Matter,” [arXiv:1712.00455 \[hep-ph\]](#).
- [41] T. Bringmann and M. Pospelov, “Novel direct detection constraints on light dark matter,” [arXiv:1810.10543 \[hep-ph\]](#).
- [42] Y. Ema, F. Sala, and R. Sato, “Light Dark Matter at Neutrino Experiments,” [arXiv:1811.00520 \[hep-ph\]](#).
- [43] B. Feldstein, P. W. Graham, and S. Rajendran, “Luminous Dark Matter,” *Phys. Rev.* **D82** (2010) 075019, [arXiv:1008.1988 \[hep-ph\]](#).
- [44] J. Hisano, K. Ishiwata, and N. Nagata, “A complete calculation for direct detection of Wino dark matter,” *Phys. Lett.* **B690** (2010) 311–315, [arXiv:1004.4090 \[hep-ph\]](#).
- [45] J. Hisano, K. Ishiwata, N. Nagata, and T. Takesako, “Direct Detection of Electroweak-Interacting Dark Matter,” *JHEP* **07** (2011) 005, [arXiv:1104.0228 \[hep-ph\]](#).
- [46] R. J. Hill and M. P. Solon, “WIMP-nucleon scattering with heavy WIMP effective theory,” *Phys. Rev. Lett.* **112** (2014) 211602, [arXiv:1309.4092 \[hep-ph\]](#).
- [47] R. J. Hill and M. P. Solon, “Standard Model anatomy of WIMP dark matter direct detection I: weak-scale matching,” *Phys. Rev.* **D91** (2015) 043504, [arXiv:1401.3339 \[hep-ph\]](#).
- [48] G. D. Kribs and E. T. Neil, “Review of strongly-coupled composite dark matter models and lattice simulations,” *Int. J. Mod. Phys.* **A31** (2016) no. 22, 1643004, [arXiv:1604.04627 \[hep-ph\]](#).
- [49] P. J. Fox, G. D. Kribs, and A. Martin, “Split Dirac Supersymmetry: An Ultraviolet Completion of Higgsino Dark Matter,” *Phys. Rev.* **D90** (2014) no. 7, 075006, [arXiv:1405.3692 \[hep-ph\]](#).

- [50] H. E. Haber and D. Wyler, “Radiative Neutralino Decay,” *Nucl. Phys.* **B323** (1989) 267–310.
- [51] **XENON100** Collaboration, E. Aprile *et al.*, “Study of the electromagnetic background in the XENON100 experiment,” *Phys. Rev.* **D83** (2011) 082001, [arXiv:1101.3866 \[astro-ph.IM\]](#). [Erratum: *Phys. Rev.*D85,029904(2012)].
- [52] D. S. Akerib *et al.*, “Radiogenic and Muon-Induced Backgrounds in the LUX Dark Matter Detector,” *Astropart. Phys.* **62** (2015) 33–46, [arXiv:1403.1299 \[astro-ph.IM\]](#).
- [53] **XENON** Collaboration, E. Aprile *et al.*, “Intrinsic backgrounds from Rn and Kr in the XENON100 experiment,” *Eur. Phys. J.* **C78** (2018) no. 2, 132, [arXiv:1708.03617 \[astro-ph.IM\]](#).
- [54] **Borexino** Collaboration, G. Bellini *et al.*, “Final results of Borexino Phase-I on low energy solar neutrino spectroscopy,” *Phys. Rev.* **D89** (2014) no. 11, 112007, [arXiv:1308.0443 \[hep-ex\]](#).
- [55] T. Appelquist *et al.*, “Detecting Stealth Dark Matter Directly through Electromagnetic Polarizability,” *Phys. Rev. Lett.* **115** (2015) no. 17, 171803, [arXiv:1503.04205 \[hep-ph\]](#).
- [56] R. Krall and M. Reece, “Last Electroweak WIMP Standing: Pseudo-Dirac Higgsino Status and Compact Stars as Future Probes,” *Chin. Phys.* **C42** (2018) no. 4, 043105, [arXiv:1705.04843 \[hep-ph\]](#).
- [57] S. P. Martin, “A Supersymmetry primer,” [arXiv:hep-ph/9709356 \[hep-ph\]](#). [Adv. Ser. Direct. High Energy Phys.18,1(1998)].
- [58] M. Cirelli, N. Fornengo, and A. Strumia, “Minimal dark matter,” *Nucl. Phys.* **B753** (2006) 178–194, [arXiv:hep-ph/0512090 \[hep-ph\]](#).
- [59] C. McCabe, “The Earth’s velocity for direct detection experiments,” *JCAP* **1402** (2014) 027, [arXiv:1312.1355 \[astro-ph.CO\]](#).
- [60] F. Mayet *et al.*, “A review of the discovery reach of directional Dark Matter detection,” *Phys. Rept.* **627** (2016) 1–49, [arXiv:1602.03781 \[astro-ph.CO\]](#).
- [61] T. Emken and C. Kouvaris, “DaMaSCUS: The Impact of Underground Scatterings on Direct Detection of Light Dark Matter,” *JCAP* **1710** (2017) no. 10, 031, [arXiv:1706.02249 \[hep-ph\]](#).
- [62] R. Rudnick and S. Gao, “4.1 - composition of the continental crust,” in *Treatise on Geochemistry (Second Edition)*, H. D. Holland and K. K. Turekian, eds., pp. 1 – 51. Elsevier, Oxford, second edition ed., 2014. <http://www.sciencedirect.com/science/article/pii/B9780080959757003016>.
- [63] H. Palme and H. O’Neill, “3.1 - cosmochemical estimates of mantle composition,” in *Treatise on Geochemistry (Second Edition)*, H. D. Holland and K. K. Turekian, eds., pp. 1 – 39. Elsevier, Oxford, second edition ed., 2014. <http://www.sciencedirect.com/science/article/pii/B9780080959757002011>.

- [64] W. McDonough, “3.16 - compositional model for the earth’s core,” in *Treatise on Geochemistry (Second Edition)*, H. D. Holland and K. K. Turekian, eds., pp. 559 – 597. Elsevier, Oxford, second edition ed., 2014.
<https://www.sciencedirect.com/science/article/pii/B9780080959757002151>.
- [65] WebElements. <https://www.webelements.com>.
- [66] T. Piffl *et al.*, “The RAVE survey: the Galactic escape speed and the mass of the Milky Way,” *Astron. Astrophys.* **562** (2014) A91, [arXiv:1309.4293](https://arxiv.org/abs/1309.4293) [[astro-ph.GA](https://arxiv.org/archive/astro)].
- [67] J. D. Lewin and P. F. Smith, “Review of mathematics, numerical factors, and corrections for dark matter experiments based on elastic nuclear recoil,” *Astropart. Phys.* **6** (1996) 87–112.
- [68] N. Spooner, *CYGNUS - a multi-latitude directional WIMP experiment*, IDM 2018.
<https://indico.cern.ch/event/699961/contributions/3056787/attachments/1694378/2726925/Spooner-CYGNUS-IDM2018v1.pdf>.
- [69] **CYGNUS** Collaboration, “CYGNO: a CYGNUS Collaboration 1 m³ Module with Optical Readout for Directional Dark Matter Search,” [arXiv:1901.04190](https://arxiv.org/abs/1901.04190) [[physics.ins-det](https://arxiv.org/archive/physics)].
- [70] **JUNO** Collaboration, Z. Djurcic *et al.*, “JUNO Conceptual Design Report,” [arXiv:1508.07166](https://arxiv.org/abs/1508.07166) [[physics.ins-det](https://arxiv.org/archive/physics)].
- [71] **Borexino** Collaboration, M. Agostini *et al.*, “A test of electric charge conservation with Borexino,” *Phys. Rev. Lett.* **115** (2015) 231802, [arXiv:1509.01223](https://arxiv.org/abs/1509.01223) [[hep-ex](https://arxiv.org/archive/hep)].
- [72] **CRESST** Collaboration, G. Angloher *et al.*, “Results on light dark matter particles with a low-threshold CRESST-II detector,” *Eur. Phys. J.* **C76** (2016) no. 1, 25, [arXiv:1509.01515](https://arxiv.org/abs/1509.01515) [[astro-ph.CO](https://arxiv.org/archive/astro)].
- [73] **PICO** Collaboration, C. Amole *et al.*, “Dark matter search results from the PICO-60 CF₃I bubble chamber,” *Phys. Rev.* **D93** (2016) no. 5, 052014, [arXiv:1510.07754](https://arxiv.org/abs/1510.07754) [[hep-ex](https://arxiv.org/archive/hep)].
- [74] **XENON100** Collaboration, E. Aprile *et al.*, “XENON100 Dark Matter Results from a Combination of 477 Live Days,” *Phys. Rev.* **D94** (2016) no. 12, 122001, [arXiv:1609.06154](https://arxiv.org/abs/1609.06154) [[astro-ph.CO](https://arxiv.org/archive/astro)].
- [75] C. Deaconu, M. Leyton, R. Corliss, G. Druitt, R. Eggleston, N. Guerrero, S. Henderson, J. Lopez, J. Monroe, and P. Fisher, “Measurement of the directional sensitivity of Dark Matter Time Projection Chamber detectors,” *Phys. Rev.* **D95** (2017) no. 12, 122002, [arXiv:1705.05965](https://arxiv.org/abs/1705.05965) [[astro-ph.IM](https://arxiv.org/archive/astro)].
- [76] **DRIFT** Collaboration, J. B. R. Battat *et al.*, “Low Threshold Results and Limits from the DRIFT Directional Dark Matter Detector,” *Astropart. Phys.* **91** (2017) 65–74, [arXiv:1701.00171](https://arxiv.org/abs/1701.00171) [[astro-ph.IM](https://arxiv.org/archive/astro)].
- [77] J. Eby, P. J. Fox, R. Harnik, and G. D. Kribs, to appear.
- [78] **SNO+** Collaboration, S. Andringa *et al.*, “Current Status and Future Prospects of the SNO+ Experiment,” *Adv. High Energy Phys.* **2016** (2016) 6194250, [arXiv:1508.05759](https://arxiv.org/abs/1508.05759) [[physics.ins-det](https://arxiv.org/archive/physics)].

- [79] **DUNE** Collaboration, R. Acciarri *et al.*, “Long-Baseline Neutrino Facility (LBNF) and Deep Underground Neutrino Experiment (DUNE),” [arXiv:1601.02984](#) [[physics.ins-det](#)].